Compact miniaturized antenna design and development for a leadless cardiac pacemaker

Abdelmouttalib Bousrout[1], Asma Khabba[2], Saida Ibnyaich[2], Tomader Mazri[1], Mohamed Habibi[3], Tole Sutikno[4]

[1]Advanced Systems Engineering Laboratory, National School of Applied Sciences, Ibn Tofail University, Kenitra, Morocco
[2]Instrumentation, Signals and Physical Systems (I2SP) Team, Faculty of Sciences SEMLALIA, Cadi Ayyad University, Marrakesh, Morocco
[3]Laboratory of Electronic Systems, Information Processing, Mechanics and Energetics, Faculty of Science, Ibn Tofail University, Kenitra, Morocco
[4]Department of Electrical Engineering, Faculty of Industrial Technology, Universitas Ahmad Dahlan, Yogyakarta, Indonesia

Article Info

ABSTRACT

Biomedical antennas play a crucial role in implantable medical telemetry, improving patient monitoring and overall well-being. This study presents a compact antenna designed for a lead-free pacemaker, with dimensions of 3.3×4×0.5 mm³. Miniaturization required open cuts in the ground plane and radiating patch, as well as a localized resistance element. The antenna features an exceptional bandwidth of 1646.8 MHz (1.0602-2.7070) GHz, guaranteeing constant performance in the human body. It covers the industrial, scientific and medical bands (ISM, 2.4-2.48 GHz) and ultra-high frequencies (UHF, 0.3-13 GHz). Simulation in a phantom produced a gain of -19.78 dBi at 2.45 GHz and -34.44 dBi at 1.2 GHz. Safety was confirmed by a specific absorption rate (SAR) study using a cardiac model. The antenna's low SAR (10 g-Avg) enabled maximum input powers to be established: 20.2 mW at 1.2 GHz and 21.23 mW at 2.45 GHz. Comparative simulations using high-frequency structure simulator (HFSS) and computer simulation technology (CST) highlighted the antenna's superiority over recent systems, demonstrating its effectiveness in the human heart. This antenna represents an advanced solution for improving patient care. Consequently, this antenna emerges as an advanced solution for addressing infectious diseases and cardiovascular conditions in the realm of medical advancements.

Corresponding Author:

Asma Khabba
Instrumentation, Signals and Physical Systems (I2SP) Team, Faculty of Sciences SEMLALIA
Cadi Ayyad University
Marrakesh, Morocco
Email: khabba.asma@gmail.com

1.   INTRODUCTION

Pacemakers are crucial implanted medical devices for individuals with bradycardia, a condition marked by a slow heartbeat. Cardiac arrest can be caused by three conditions related to slow heart rhythm: heart tissue damage, hypertrophic cardiomyopathy, and syncope. With over 5 million Americans and 25 million people worldwide affected by heart ailments, the number of pacemakers installed has exceeded 3 million [1]. Traditional pacemakers have advanced significantly since the first one was successfully implanted in a patient in 1958 [2]. The wireless cardiac pacemaker system, as seen in Figure 1, makes use of antennas to provide patients streamlined and integrated medical features. Real-time monitoring and safety procedures are crucial for maintaining the best operation of a wireless cardiac pacemaker device. A number

of important aspects are at play in this situation, including component downsizing, lifespan, and the pacemaker system's amount of built-in medical communication [3]. Consequently, the study of implanted antennas for wireless pacemaker systems remains crucial for the scientific community. Medical electronic equipment and the radio transmission of information both have specific frequency allotments established by the International Telecommunication Union (ITU).
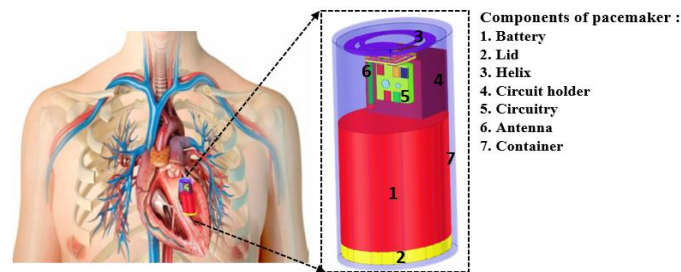

Figure 1. Configuration of the leadless pacemaker and its constituent elements

In the realm of medical implants, this spectrum allocation ensures a consistent resource for radio signal transmission. The most commonly utilized frequency bands for implantable antennas include the 402–405 MHz range designated for the implantable medical communication service (MICS), the 1.395–1.4 GHz range for the wireless medical telemetry service (WMTS), and the industrial, scientific, and medical (ISM) bands, which cover the 433–434 MHz, 902–908 MHz, 2.4–2.48 GHz, and 5.715–5.875 GHz ranges. Additionally, the ultra-high frequency (UHF) band spans from 0.3 GHz to 13 GHz. To ensure high-quality transmission, the use of ultra-wideband (UWB) frequencies, ranging from 3.1 GHz to 10.6 GHz, has been authorized in several international regions. The med radio frequency band, which extends from 401 to 406 MHz, is widely used for wireless implanted devices, however sources have indicated that antennas operating in this frequency range have limited bandwidths, resulting in low data rates and limited image resolution [4], [5].

The field of medically implanted antennas has seen significant developments recently. One area of particular interest is the elements that affect radio wave propagation within the human body, as discussed in reference [6]. Recent years have seen the proposal of several implanted antenna devices, mostly for telemetry applications. A compact antenna configuration featuring two communication channels at 915 MHz and 2.45 GHz was developed in order to track intracranial pressure (ICP), according to [7]. The proposed antenna demonstrated exceptional broadband performance and gain at both targeted frequencies. In a previous investigation [8], an implanted multiple-input multiple-output (MIMO) antenna operating at 2.45 GHz was highlighted, achieving a peak gain of -15.18 dBi. Despite its adequate gain, the complexity introduced by its four ports could hinder its compatibility with modern implantable medical devices (IMDs). Another study by Bashir *et al.* [9] presented an implanted antenna with a volume of 9.8 mm³, designed to function within the ISM band (2.40-2.48 GHz) for gastrointestinal endoscopy applications. This antenna exhibited a gain of -12 dBi and an impedance bandwidth of 483 MHz; however, its larger size rendered it unsuitable for smaller implants such as wireless leadless pacemakers. Moreover, a separate effort [10] detailed the development of a compact dual-band antenna, measuring 7.2×0.2 mm³, intended for use in implanted batteries. This antenna demonstrated maximum gains of -25.65 dBi at 928 MHz and -28.44 dBi at 2.45 GHz on a single-layer skin phantom, although it exceeded the allowable specific absorption rate (SAR) limits [11], [12]. In the realm of biomedical engineering, the quest for optimal implantable antennas has driven various advancements tailored to specific applications. For instance, within the 2.4 GHz ISM band, a circularly polarized (CP) implantable antenna was developed for cardiac pacemakers [13]. Despite its impressive characteristics, including a gain of -15.87 dBi and an 890 MHz bandwidth, its large dimensions of 40×40×1.27 mm³ posed a significant drawback.

In another study by Zada and Yoo [14], a triple-band implantable antenna was designed to cater to a range of biomedical requirements, covering ISM frequencies at 915 MHz and 2.45 GHz, along with the mid-field band from 1824 to 1980 MHz. However, this antenna displayed narrower bandwidths and reduced gain across both ISM and mid-field bands. Similarly, a dual-band implantable antenna aimed at operating within the ISM and MedRadio bands was introduced in [15]. Despite its debut, this antenna faced challenges related to insufficient bandwidth and a considerable physical footprint.

Attention shifted towards a single-band implantable antenna tailored for glucose monitoring within the ISM band (2.4−2.48 GHz), boasting a remarkable gain of -17 dBi [16]. Nonetheless, its voluminous size of 91.7575 mm³ and limited bandwidth of 300 MHz posed practical constraints. The pursuit of innovation led to the proposal of a uniquely shaped antenna, primarily targeted for pacemaker applications, capable of operating within ISM and MICS bands [17]. However, its complex geometry, large dimensions, and modest gain values underscored the need for further refinement. Subsequently, Saha *et al.* [18] introduced a CP antenna tailored for bio-telemetry applications, featuring a compact form factor measuring 10×10×0.3 mm³ and simulated gain reaching 7.79 dBi across its operational frequency band. Despite its promising attributes, the suitability of single-band antennas for integrated wireless medical devices (IWMDs), encompassing wireless charging, activation, and bio-telemetry functionalities, remains under scrutiny [19].

In a recent scholarly publication [20], a MIMO antenna specifically tailored for high data-rate biomedical applications was introduced by researchers. Despite demonstrating commendable gain, the antenna exhibited limitations in terms of bandwidth, physical dimensions, and isolation. Similarly, another academic investigation detailed in [21] presented a circular dual-band implanted antenna featuring a radiating slot patch. The primary objective was to enhance power transfer connectivity, achieved through the inclusion of an external metallic reflector positioned beneath the user's arm. Furthermore, Iqbal *et al.* [22] emphasized the discovery of a self-duplexing implantable antenna equipped with dual ports. Distinguished by its intricately engineered design, this antenna minimized physical footprint while concurrently serving the dual purpose of data transmission and RF energy harvesting.

These inquiries underscore the inherent complexities associated with antenna design for biomedical applications spanning diverse frequency ranges, posing challenges to their seamless integration into IMDs. Consequently, a compelling need arises for further research efforts focused on the development of an implantable antenna characterized by optimal efficiency. Such an antenna should embody attributes including compact volume, elevated gain, extensive bandwidth, minimal SAR, and dependable telemetric capabilities.

The current investigation endeavors to develop an ultrawideband implantable antenna tailored for a lead-free pacemaker. The proposed antenna, occupying dimensions of 3.3×4×0.5 mm³, is engineered to encompass the ISM bands spanning 2.4-2.48 GHz, as well as UHF ranging from 0.3 to 13 GHz. Several downsizing techniques were used to maximize performance using a small structure that included a ground plane and radiating element integrated into the substrate and superstrate layers of the leadless cardiac pacemaker (LCP) Rogers ULTRALAM. Rectangular open-ended slots and a resistor element are incorporated to increase electrical length, support impedance, and widen the bandwidth within the intended frequency range. Initial design and analysis were conducted utilizing a homogeneous phantom (HSP) measuring 100×100×100 mm, facilitated by high-frequency structure simulator (HFSS) software. Subsequent validation of the antenna's efficacy encompassed simulations in heterogeneous mediums mimicking diverse human body tissues, alongside the inclusion of implantable device components. To corroborate findings, the proposed antenna underwent re-simulation via the computer simulation technology (CST) simulator. Notably, the structure exhibited an impedance-matched bandwidth of 1646.8 MHz, with a peak gain of -19.78 dBi at 2.45 GHz and -34.44 dBi at 1.2 GHz, thereby manifesting omnidirectional radiation characteristics. Safety scrutiny, focusing on SAR, affirmed the antenna's suitability for application. Leveraging its high-gain attributes, a dependable communication range of 14 m was established, achieving a bit rate of 78 Mbps through meticulous link budget calculations.

This article is structured as follows: the introduction explores the significance of biomedical implants, emphasizing the radio component. It outlines the requirements, challenges, and contributions from prior works in this domain, setting the context for our study. The second part details the procedures and methods used in designing the proposed implanted antenna, including the simulation environment and parametric study results. We also address coupling effects arising from integrating the antenna into relevant implants, such as pacemakers and endoscopic capsules. The subsequent section focuses on studying SAR using a phantom model in a homogeneous environment. The final section analyzes the link budget for the proposed antenna, featuring a comparative study, concluding remarks, and references.

2. METHOD
2.1. Designing the intended antenna and its associated system configuration

The provided description pertains to an ultra-miniaturized UWB antenna, measuring a compact 3.3×4×0.5 mm³. Figures 2(a) to (c) depicts the antenna top view, antenna bottom view, and antenna exploded view, respectively. This antenna design adopts a small meander-shaped patch configuration, offering a low-profile form factor conducive to seamless circuit integration. Notably, it exhibits suitability for integration within wireless pacemakers. The antenna's surface area is purposefully minimized by incorporating intricate meander-shaped slots within the radiating patch, thereby elongating the path of surface currents. This decision is consistent with the usage of spiral and meander antennas because of their intrinsic dispersion

qualities, which make them less vulnerable to changes in the dielectric characteristics of the biological tissues around them [23]. Notably, well-placed strategic perforations in the ground plane improve the antenna's performance and bandwidth even further. The coaxial feed has a thin 0.46 mm diameter and is strategically placed close to the patch antenna's upper central section. The substrate consists of a 0.25 mm thick layer of Rogers TMM 10 material, notable for its tangent loss coefficient of 0.0022 and dielectric constant of 9.2. To prevent direct contact with physiological tissues, all components, including the antenna, are encapsulated in alumina ceramic (Al_2O_3). Furthermore, employing a biocompatible ceramic superstrate helps reduce the antenna's size and expand its operational bandwidth [24].
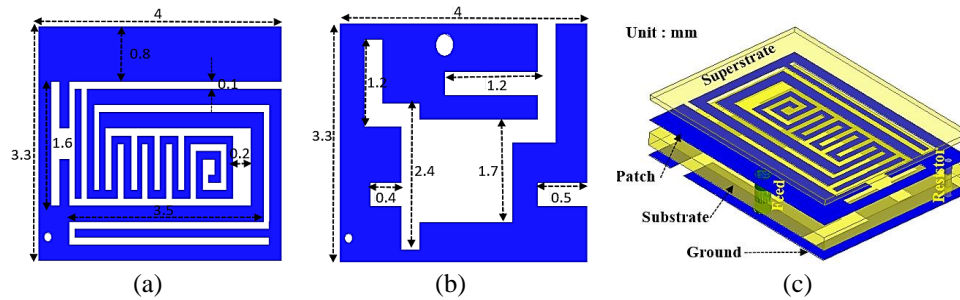
Figure 2. Configuration and design parameters of the proposed antenna; (a) antenna top view, (b) antenna bottom view, and (c) antenna exploded view

It is essential to recognize that implantable antennas operate in conjunction with other interconnected components, rather than in isolation, in real-world applications. The proposed antenna has been meticulously designed in our research project to integrate seamlessly into wireless pacemakers. Figure 1 illustrates this seamless integration of the proposed antenna into wireless pacemakers.

The essential components of the LCP include electrodes, circuit holders, antennas, containers, circuits, batteries, and covers. While the circuit carrier is made of Rogers RT/duroid 6010 material, the electrodes, circuits and batteries are represented in the simulations as perfect electrical conductors. Other biomedical implant models can be found in the literature; these models are distinguished by architectures that may resemble or differ from the one we have proposed. However, our main objective is to better understand the complex interactions that take place between the antenna and these numerous medical devices. Our main concerns are twofold: firstly, to proactively identify any potential effects on the antenna's performance and, secondly, to create a safety net to guarantee its flawless operation under real-world constraints.

2.2. Designing steps

As depicted in Figure 3, the proposed wideband antenna underwent a structured and iterative four-stage optimization and development process. Figure 4 presents the reflection coefficient (S11) results corresponding to each stage. The design evolution proceeded incrementally, beginning with a basic antenna configuration that included slots in both the radiator and the ground plane.
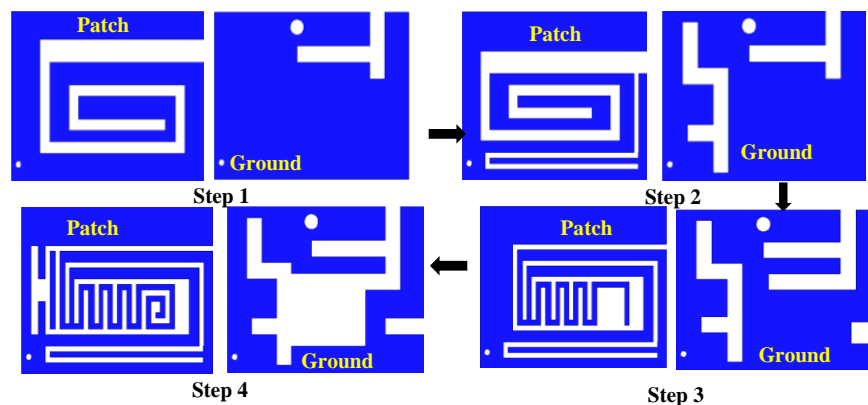

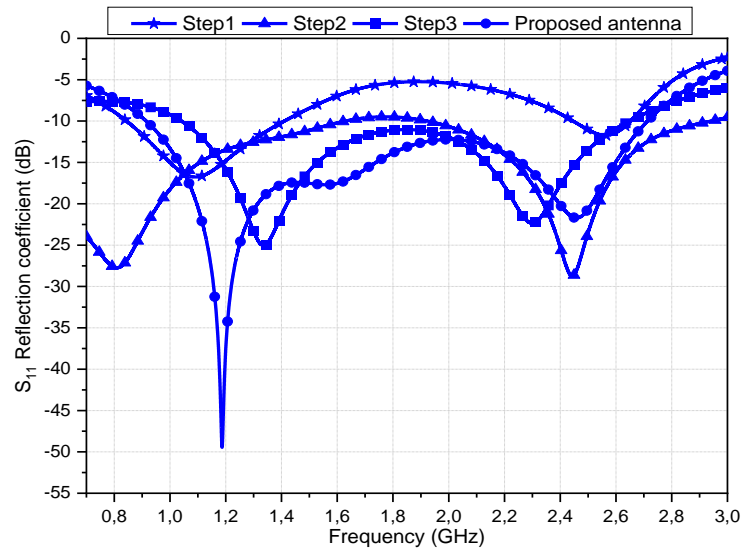Figure 3. Designing steps of the UWB antenna

Figure 4. Reflection coefficient for each designing steps

During the first phase, a reflection coefficient of -15 dBi was found for a single weak resonance at 1.48 GHz. In the second step, more slots were precisely added to the ground plane and patch. This resulted in the formation of a secondary resonance at 2.8 GHz with an S11 value of -9.98 dBi. In the third phase, a rectangular cut-out and more slots were added to the ground plane. Due to these changes, the previously identified 2.8 GHz resonance has moved to 2.38 GHz. Additionally, careful adjustments brought the lower resonance frequency into alignment with the desired 1.4 GHz frequency. This frequency modulation can be attributed to the increased capacitance resulting from the incorporation of slots in either the patch or the ground plane, consistent with expected trends. The fourth and final stage marked the culmination of these developmental enhancements.

Consequently, two distinct resonances were achieved: a lower resonance at 1.41 GHz with an S11 value of -50 dBi, and an upper resonance at approximately 2.45 GHz with a reflection coefficient of -26 dBi. This concerted progression resulted in the attainment of an exceptionally broad bandwidth of 1836.8 MHz.

2.3. Parametric study

A thorough examination of key design parameters, including the feed point location, resistor placement, and its resistance value, is crucial for optimizing the proposed antenna's configuration. This section emphasizes the necessity of a parametric study to achieve the ultimate antenna design.

2.3.1. Impacts of the position of the feed

Figure 5 illustrates the impact of the feeding location on the S_{11} parameter. Clearly, the strategic positioning of the power supply point has a considerable influence on improving impedance matching and optimizing dual-band operation. When the power supply is located at point P1, a subtle resonance in the low-frequency range appears, characterized by an S_{11} level of -17.6 dB, covering a bandwidth of 550 MHz centered on 1.1 GHz. At the same time, there is a distinctive high-frequency resonance at 2.26 GHz, albeit associated with a high S11 value. When the antenna is excited at point P2, the impedance matching challenge persists; however, there is an improvement in the S_{11} level associated with the high-frequency resonance. Nevertheless, when the antenna is excited first at point P3 and subsequently at point P4, a more pronounced alignment with the resonance frequency becomes evident. Our comprehensive investigation leads to the conclusion that the optimal feeding location, for improved alignment with significant bandwidths, corresponds to point P4.

2.3.2. The impact of changing the values and position of introducing resistor

One of the key parameters in determining the right bandwidth for the required antenna is the value of the resistor element and its location. This contributes to improved performance and a substantial reduction in size. Figure 6 illustrates the reflection coefficient as a function of different feed resistor positions. The matching performance of the antenna exhibits a strong dependence on the resistor's placement. Initially, in the first resistor position, impedance matching falls short, causing the resonant frequencies to deviate from the expected range. Nevertheless, it is noteworthy that both low and high resonance coefficients remain

below the -10 dB threshold, which is acceptable. In the second position, the antenna undergoes a significant improvement, aligning the frequencies more closely with the desired values. Specifically, the reflection coefficient values at 1.25 GHz and 2.45 GHz measure -28 dB and -18 dB, respectively.
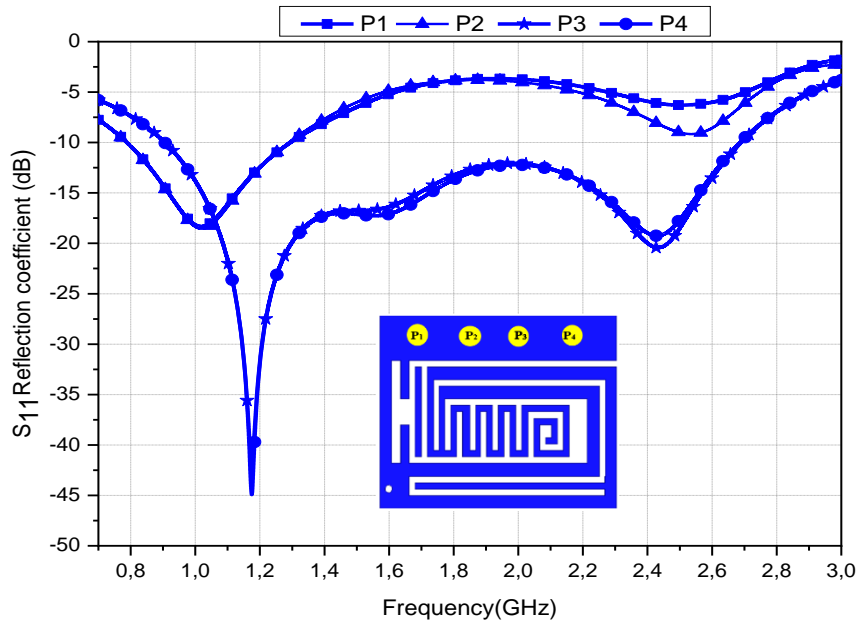

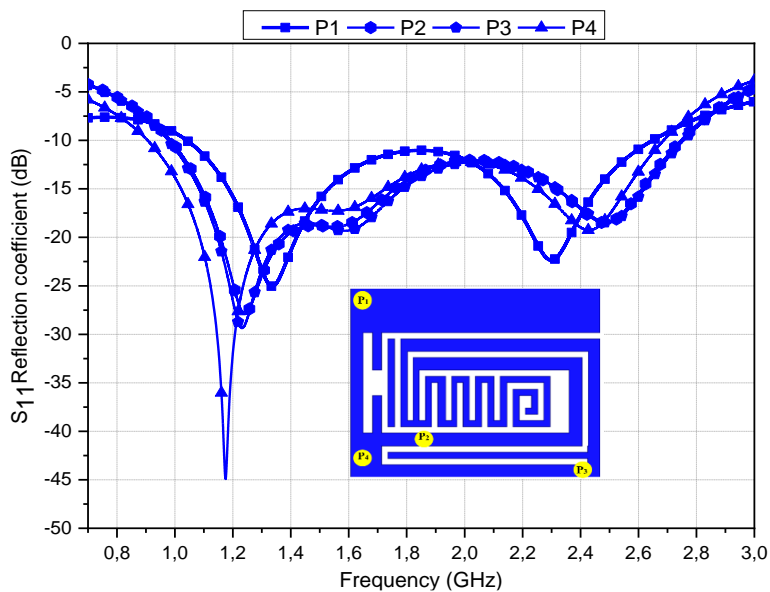Figure 5. Effect on S_{11} due to variations in feed position

Figure 6. Effect of varying the position of the resistor

Ultimately, relocating the resistor from the third to the fourth position, as depicted in Figure 6, attains the targeted frequency band. This positioning yields a well-matched antenna performance, with reflection coefficient values of -45 dB and -20 dB at 1.2 GHz and 2.43 GHz, respectively. Upon establishing the resistor's position, the determination of its value becomes imperative. Figure 7 illustrates the comparison of reflection coefficients for different resistor values connecting the lower patch to ground through the substrate. The results underscore that higher resistance values lead to a shift of the resonant frequency towards lower frequency ranges, emphasizing the substantial impact of resistance on the operational

frequency band. The findings in Figure 7 validate the preference for a 5 ohm resistor, identified as the optimal choice for achieving a satisfactory bandwidth.
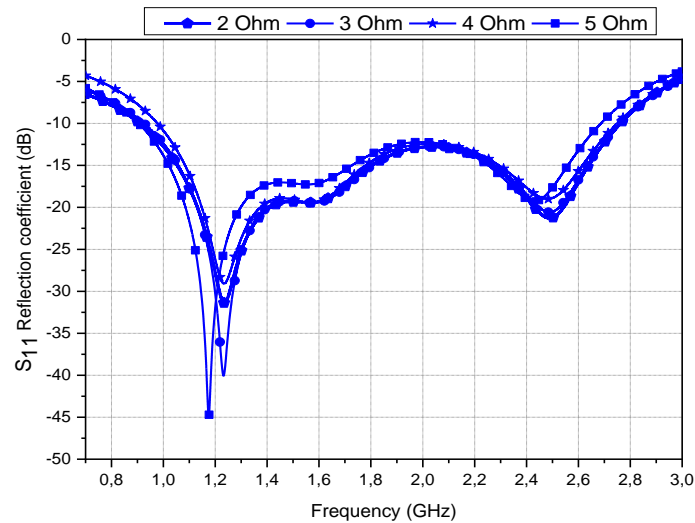

Figure 7. Effect of varying values of the resistor

2.4. Simulation and environments

The initial phase of antenna development involved a meticulous process of modeling and optimization within a uniform box phantom designed to closely resemble the dimensions of the human heart, as illustrated in Figure 8. This analytical procedure was executed through the utilization of the Ansoft HFSS software. Furthermore, to ensure accuracy, the electromagnetic characteristics of the heart tissue, specifically its conductivity and dielectric permittivity, were considered, amounting to 2.215 S/m and 54.918, respectively [25], in the context of a working frequency of 2.4 GHz. To corroborate and validate the results obtained from the parametric sensitivity analysis conducted with HFSS, a second simulation was conducted using CST. This additional simulation was carried out on the same phantom model, thus serving as a means to establish the reliability and correlation of the outcomes derived from the preceding analysis.
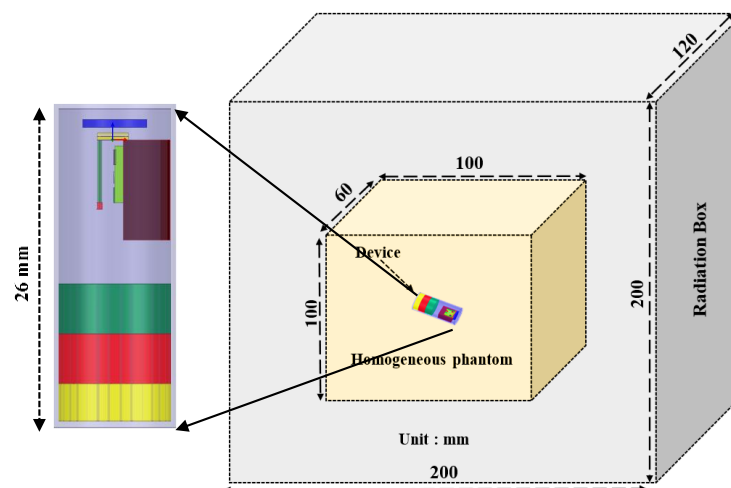

Figure 8. Simulation setup for the proposed antenna and associated system

3.   RESULTS AND DISCUSSION

When implantable antennas are coupled with IMDs, significant detuning issues arise. In response to the challenge of mitigating frequency detuning, the exploration of UWB antennas has emerged as a viable

solution [8]. The primary aim of this research endeavor revolved around the development of a highly compact antenna that would exhibit coherent impedance matching across an exceptionally broad bandwidth. The application context for this proposed antenna design necessitated optimal operational performance as it was intended for use deep within the human body. The (HFSS, version 2022.R2) was used to optimize the suggested antenna arrangement within a homogenous phantom as the first step in the research process. The antenna was then put through simulation using CST Microwave Studio. In the setting of the homogenous cardiac environment. Figures 9(a) and (b) illustrates the Far-Field polar gain pattern at 2.4 GHz and 1.2 GHz, respectively, for both Planes E and H. Surprisingly, these patterns behaved almost exactly the same way regardless of the situation.
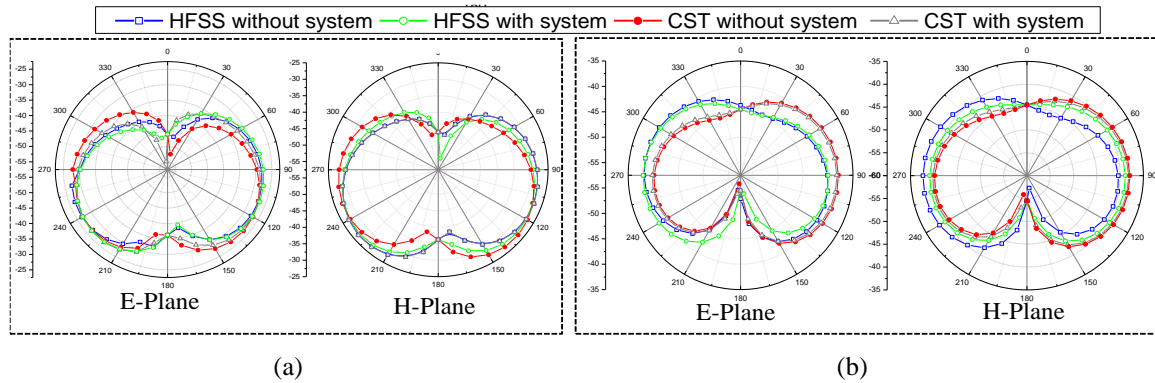
Figure 9. Far-field polar gain pattern comparison at; (a) 2.4 GHz and (b) 1.2 GHz

Through HFSS simulations, the peak gains at the specified frequencies of 1.2 GHz and 2.45 GHz were determined to be -36.77 dBi and -37.1 dBi, respectively. Accordingly, at the aforementioned frequencies, CST simulations produced peak gains of -25.62 dBi and -25.8 dBi. The research also focused on coupling issues between the proposed antenna and the device parts, both of which are located in close proximity to each other. The main objective was to understand the antenna's ramifications and sensitivity to coupling-induced phenomena such as interference and signal degradation. Designers were able to make judicious choices thanks to simulations created to study these complex links in depth. According to the results shown in Figure 10, coupling effects have no impact on the performance of the proposed antenna, guaranteeing reliable system operation. Clearly, the proximity of the antenna to the implant has no effect on the matching quality. This in-depth coupling analysis significantly enhances overall system performance and reliability, thanks to the harmonious integration of antenna and device components.
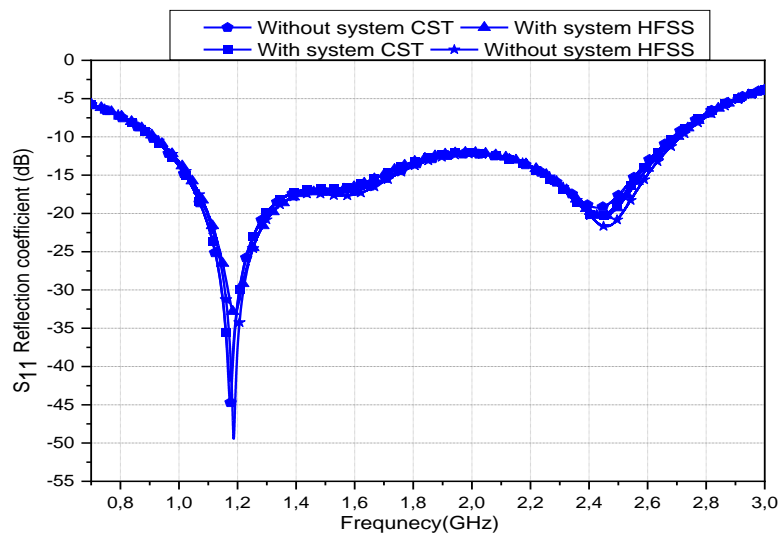

Figure 10. Impact of metallic system components on performance of the proposed antenna due to coupling effects

Inside the right ventricle is the ideal place for the antenna in terms of patient therapy. Considering the effects of radiation on cardiac tissue, as measured by the SAR, is crucial in light of this. It is imperative to comply with established safety limits by ensuring that the SAR values for 1 g and 10 g of tissue stay below 1.6 W/kg and 2 W/kg, respectively [19]. To solve this issue, numerical studies have been performed with a homogeneous cardiac model to find the SAR limits and maximum permissible power (MAP) limitations that satisfy these requirements. Figures 11(a) and (b) illustrate the modeling results of the 10-g SAR distribution for the antenna operating at 1.2 GHz with input powers of 1 W and 21.23 mW, respectively. Similarly, the simulation of the 10-g SAR distribution for the antenna at 2.4 GHz with input power of 1 W and 22.20 mW, respectively, is shown in Figures 12(a) and (b). There were two different maximums for the allowed input power: 20.20 mW and 21.23 mW. The calculated SAR values for 1.2 GHz and 2.45 GHz are listed in Table 1.
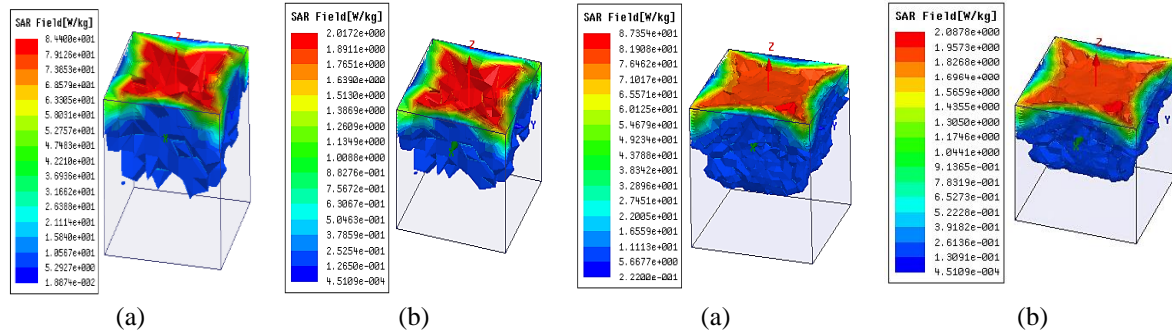

| (a) | (b) | (a) | (b) |

Figure 11. Simulating the distribution of 10-g SAR for the antenna at 1.2 GHz with input power of; (a) 1 W and (b) 21.23 mW

Figure 12. Simulating the distribution of 10-g SAR for antenna at 2.4 GHz with input power of; (a) 1 W and (b) 20.20 mW

Table 1. Maximum SAR values and allowable maximum input powers for 1-watt input power

Frequency (GHz)	Tissue model	SAR (W/kg)		Max allowable input power (mW)	
		10 g-Avg	1 g-Avg	10 g SAR limit	1 g SAR limit
2.45	Heart	87.35	798.21	20.20	2.62
1.2		84.00	691.1	21.23	2.21

Ensuring the accurate determination of telemetry range between the external base station and the implantable device is paramount for the reliable transmission of biological data. However, achieving this entails intricate computations encompassing various losses, such as cable losses, free space losses, and losses associated with impedance mismatches and antenna materials [26]. The Friis equation serves as the foundation for calculating link margins by assessing the disparity between antenna power (AP) and required antenna power (RP). Maintaining a connection margin exceeding 20 dB is critical to ensuring robust communication. Table 2 presents a comprehensive breakdown of the essential parameters utilized in these computations. In (1) delineates the RP calculation:

$$R_p = B_r + \frac{E_b}{N_0} + KT \tag{1}$$

Here, E_b/N_0, K, T_o, and B_r stand for temperature, bit rate, phase shift keying, and Boltzmann's constant, in that order. On the other hand, A_p can be computed using (2):

$$A_p(dB) = P_{TX} + G_{TX} + G_{RX} - L_f - P_L \tag{2}$$

where the initials P_{TX}, G_{TX}, and G_{RX} stand for transmitter power, transmitter antenna gain, and implanted receiver antenna gain, respectively. Free space and polarization mismatch losses are represented by the letters L_f and P_L, respectively. The distance (d) between the broadcast and receive antennas determines L_f in most cases. In (3) can be used to calculate this loss.

$$L_f(dB) = 10\delta \log\left(\frac{d}{d_0}\right) + 10 \log\left(\frac{4\pi d_0}{\lambda_0}\right)^2 + S_{(dB)} \tag{3}$$

Table 2. Key parameters taken into consideration for conducting a link budget analysis

Parameters	Variables	Values
Resonance frequency	f_0 (GHz)	1.2-2.4
Noise power density	N_0 (dB/Hz)	-203.93
Transmitter power	P_{TX} (dB_m)	-16
Polarization mismatch loss	P_L (dB)	1
Temperature	T_0 (Kelvin)	273
Path loss	L_f (dB)	Distance dependent
Transmitter antenna gain	G_{TX} (dB_i)	G_{TX}(1.2 GHz) =−34.44 dBi
		G_{TX}(2.4 GHz) = −19.78 dBi
Receiver antenna gain	G_{RX} (dB_i)	G_{RX} = 2 dBi
Boltzmann constant	K	1.38×10^{-23}
Available power	A_P (dB)	Distance dependent
Bit rate	B_r	78 bits
Required power	R_P (dB)	Adaptive (bit rate)
Antenna power	A_P (dB)	Adaptive (distance)
Path loss exponent	δ	1.5
Shadowing effect	S(dB)	0

The formula for link margin involves several variables, including d for distance between antennas, δ for path loss exponent, λ_0 for wavelength in free space, and d_0 for reference distance calculated as $d_0 = \frac{2L^2}{\lambda_0}$, L is the maximum dimension of the antenna in the direction of radiation. Additionally, S represents random dispersion about the mean. The value of δ depends on the propagation environment, for indoor propagation, $\delta=2$, while for open space propagation $\delta=1$ [27].

Ensuring patient safety, it's imperative to note that the European Research Council imposes a limit on input power, capping it at 25 W. Issues concerning the availability of batteries and circuits with dynamic medical implants (DMI) capabilities are pivotal considerations. The possibility of skin implantation is also being considered, depending on how the suggested antenna will be used and how much power it will require. The bit rate Br of the suggested antenna is set at 78 Mbps, while the transmitted power Pt anticipated in the context of skin implantation devices is set at -16 dBm. Figure 13 shows that with an input power of -16 dBm, data transmission at a data rate of 78 Mbps can be accomplished across a distance of more than 15 m for the 1.2 GHz frequency and up to 13 m for the 2.4 GHz frequency. The transmission range is naturally impacted by variations in data rate.
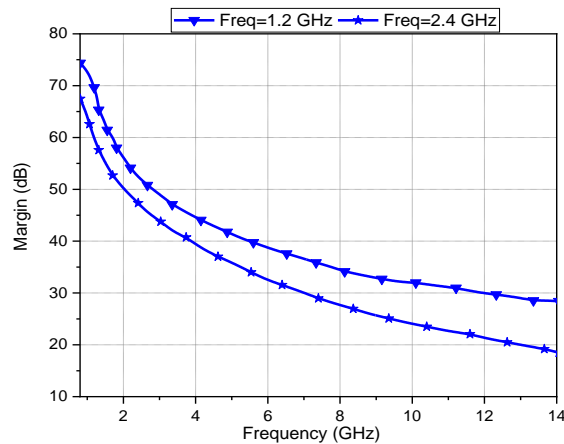

Figure 13. Link budget analysis conducted for the antenna within an HSP

The comparative study results presented in Table 3 highlight the advantages of the suggested antenna with respect to patient safety, regarding volume, antenna material, gain, bandwidth, SAR, and structural simplicity. The suggested antenna clearly outperforms the work cited in [4], [21], demonstrating twice the bandwidth and better performance. This benefit is ascribed to its flexible structure, straightforward geometry, and compact form, all of which promote smooth integration. The suggested antenna keeps a larger

bandwidth than the references [4], [8], [26] even if its SAR values are slightly greater than those of the reference antenna [4]. Furthermore, the antenna design incorporates sensors, batteries, and electronic parts.

Table 3. Proposed antenna comparison with recent works

Ref.	Volume (mm³)	Freq. (GHz)	Bandwidth (MHz)	Gain (dBi)	SAR (W/kg)		Device study?
					10 g-Avg	1 g-Avg	
[4]	3×3×0.5	2.45	528	-24.9	32.3	10.8	Yes
[26]	7×7×0.2	0.915	107.5	-27.65	89.70	730.07	Yes
		2.45	560	-22.99	82.71	591.4	
[8]	18.5×18.5×1.27	2.45	440	-15.99	-	-	No
[27]	9.2×9.2×0.5	2.4-4.8-5.8	6387-625-156-344	-15.8/-15.2/-16.6/-15.8	$(350.8\text{-}97.9\text{-}205\text{-}156)_{1g}$		Yes
[28]	5×5×0.635	1.4-2.45	300	-27.68	81.7	767	Yes
			380	-27.10	84.6	785	
[29]	7×7×0.2	0.915-2.45	1174-2333	-27.65/-22.99	$(730.07\text{-}591.40)_{1g}$		Yes
[30]	7×7×0.254	0.915	−28	21.85	8.1_{1g}		No
[31]	31.5×15×0.787	**3.3**	1500	-18.5	-		No
This work	3.3×4×0.5	1.2	1646.8	-34.44	84.0	691.1	Yes
		2.45		-19.78	87.35	798.21	

4.　CONCLUSION

　　　This paper introduced a wideband implantable antenna designed to operate at 1.2 and 2.45 GHz, with a focus on biomedical applications, specifically for a LCP. Miniaturization techniques, including the addition of a resistor element and rectangular slots to the ground plane, were employed to optimize key parameters. The final design achieved a remarkably compact volume of 3.3×4×0.5 mm³. Furthermore, the outcomes of the SAR study confirm that the suggested antenna can be implanted safely in patients. Key features of the antenna are its omnidirectional radiation pattern, high gain, optimum impedance matching, ultra-compact dimensions, broad bandwidth, patient safety, and biotelemetric capability. Furthermore, comparison analysis highlights how much better the proposed antenna performs than current cutting-edge implantable antennas.

REFERENCES

[1] H. G. Mond and A. Proclemer, "The 11th World Survey of Cardiac Pacing and Implantable Cardioverter-Defibrillators: Calendar Year 2009–A World Society of Arrhythmia's Project," *Pacing and Clinical Electrophysiology*, vol. 34, no. 8, pp. 1013–1027, 2011, doi: 10.1111/j.1540-8159.2011.03150.x.

[2] D. S. Chew and V. Kuriachan, "Leadless cardiac pacemakers," *Current Opinion in Cardiology*, vol. 33, no. 1, pp. 7–13, 2018, doi: 10.1097/hco.0000000000000468.

[3] F.-J. Huang, C.-M. Lee, C.-L. Chang, L.-K. Chen, T.-C. Yo, and C.-H. Luo, "Rectenna Application of Miniaturized Implantable Antenna Design for Triple-Band Biotelemetry Communication," *IEEE Transactions on Antennas and Propagation*, vol. 59, no. 7, pp. 2646–2653, 2011, doi: 10.1109/tap.2011.2152317.

[4] Y. Feng, Z. Li, L. Qi, W. Shen, and G. Li, "A compact and miniaturized implantable antenna for ISM band in wireless cardiac pacemaker system," *Scientific reports*, vol. 12, no. 1, p. 238, Jan. 2022, doi: 10.1038/s41598-021-04404-3.

[5] M. Yousaf *et al.*, "Compacted Conformal Implantable Antenna With Multitasking Capabilities for Ingestible Capsule Endoscope," *IEEE Access*, vol. 8, pp. 157617–157627, 2020, doi: 10.1109/access.2020.3019663.

[6] M. M. Soliman *et al.*, "Review on Medical Implantable Antenna Technology and Imminent Research Challenges," *Sensors (Basel, Switzerland)*, vol. 21, no. 9, p. 3163, May 2021, doi: 10.3390/s21093163.

[7] F. Faisal, M. Zada, A. Ejaz, Y. Amin, S. Ullah, and H. Yoo, "A Miniaturized Dual-Band Implantable Antenna System for Medical Applications," *IEEE Transactions on Antennas and Propagation*, vol. 68, no. 2, pp. 1161–1165, 2020, doi: 10.1109/tap.2019.2938591.

[8] Y. Fan, J. Huang, T. Chang, and X. Liu, "A Miniaturized Four-Element MIMO Antenna With EBG for Implantable Medical Devices," *IEEE Journal of Electromagnetics, RF and Microwaves in Medicine and Biology*, vol. 2, no. 4, pp. 226–233, 2018, doi: 10.1109/jerm.2018.2871458.

[9] Z. Bashir *et al.*, "A Miniaturized Wide Band Implantable Antenna for Biomedical Application," *2019 UK/ China Emerging Technologies (UCET)*. IEEE, 2019, doi: 10.1109/ucet.2019.8881849.

[10] F. Faisal and H. Yoo, "A Miniaturized Novel-Shape Dual-Band Antenna for Implantable Applications," *IEEE Transactions on Antennas and Propagation*, vol. 67, no. 2, pp. 774–783, 2019, doi: 10.1109/tap.2018.2880046.

[11] "IEEE Standard for Safety Levels with Respect to Human Exposure to Electric, Magnetic, and Electromagnetic Fields, 0 Hz to 300 GHz - Corrigenda 2." IEEE, doi: 10.1109/ieeestd.2020.9238523.

[12] "IEEE Standard for Safety Levels with Respect to Human Exposure to Radio Frequency Electromagnetic Fields, 3 kHz to 300 GHz." IEEE, doi: 10.1109/ieeestd.2006.99501.

[13] Z.-J. Yang, L. Zhu, and S. Xiao, "An Implantable Circularly Polarized Patch Antenna Design for Pacemaker Monitoring Based on Quality Factor Analysis," *IEEE Transactions on Antennas and Propagation*, vol. 66, no. 10, pp. 5180–5192, 2018, doi: 10.1109/tap.2018.2862242.

[14] M. Zada and H. Yoo, "A Miniaturized Triple-Band Implantable Antenna System for Bio-Telemetry Applications," *IEEE Transactions on Antennas and Propagation*, vol. 66, no. 12, pp. 7378–7382, 2018, doi: 10.1109/tap.2018.2874681.

[15] Y. Cho and H. Yoo, "Miniaturised dual-band implantable antenna for wireless biotelemetry," *Electronics Letters*, vol. 52, no. 12, pp. 1005–1007, 2016, doi: 10.1049/el.2016.1051.

[16] X. Y. Liu, Z. T. Wu, Y. Fan, and E. M. Tentzeris, "A Miniaturized CSRR Loaded Wide-Beamwidth Circularly Polarized Implantable Antenna for Subcutaneous Real-Time Glucose Monitoring," *IEEE Antennas and Wireless Propagation Letters*, vol. 16, pp. 577–580, 2017, doi: 10.1109/lawp.2016.2590477.

[17] M. Kod *et al.*, "Feasibility Study of Using the Housing Cases of Implantable Devices as Antennas," *IEEE Access*, vol. 4, pp. 6939–6949, 2016, doi: 10.1109/access.2016.2613968.

[18] P. Saha, D. Mitra, and S. K. Parui, "A circularly polarised implantable monopole antenna for biomedical applications," *Progress In Electromagnetics Research C*, vol. 85, pp. 167–175, 2018, doi: 10.2528/pierc18051807.

[19] Z. Bao, Y.-X. Guo, and R. Mittra, "Single-Layer Dual-/Tri-Band Inverted-F Antennas for Conformal Capsule Type of Applications," *IEEE Transactions on Antennas and Propagation*, vol. 65, no. 12, pp. 7257–7265, 2017, doi: 10.1109/tap.2017.2758161.

[20] A. Iqbal, M. Al-Hasan, I. Ben Mabrouk, and M. Nedil, "A Compact Implantable MIMO Antenna for High-Data-Rate Biotelemetry Applications," *IEEE Transactions on Antennas and Propagation*, vol. 70, no. 1, pp. 631–640, 2022, doi: 10.1109/tap.2021.3098606.

[21] S. Ding, S. Koulouridis, and L. Pichon, "Implantable Wireless Transmission Rectenna System for Biomedical Wireless Applications," *IEEE Access*, vol. 8, pp. 195551–195558, 2020, doi: 10.1109/access.2020.3032848.

[22] A. Iqbal, M. Al-Hasan, I. Ben Mabrouk, A. Basir, M. Nedil, and H. Yoo, "Biotelemetry and Wireless Powering of Biomedical Implants Using a Rectifier Integrated Self-Diplexing Implantable Antenna," *IEEE Transactions on Microwave Theory and Techniques*, vol. 69, no. 7, pp. 3438–3451, 2021, doi: 10.1109/tmtt.2021.3065560.

[23] S. Kim and H. Shin, "An Ultra-Wideband Conformal Meandered Loop Antenna for Wireless Capsule Endoscopy," *Journal of Electromagnetic Engineering and Science*, vol. 19, no. 2, pp. 101–106, 2019, doi: 10.26866/jees.2019.19.2.101.

[24] H.-Y. Lin, M. Takahashi, K. Saito, and K. Ito, "Performance of Implantable Folded Dipole Antenna for In-Body Wireless Communication," *IEEE Transactions on Antennas and Propagation*, vol. 61, no. 3, pp. 1363–1370, 2013, doi: 10.1109/tap.2012.2227099.

[25] S. Gabriel, R. W. Lau, and C. Gabriel, "The dielectric properties of biological tissues: II. Measurements in the frequency range 10 Hz to 20 GHz," *Physics in Medicine and Biology*, vol. 41, no. 11, pp. 2251–2269, 1996, doi: 10.1088/0031-9155/41/11/002.

[26] S. A. A. Shah and H. Yoo, "Scalp-Implantable Antenna Systems for Intracranial Pressure Monitoring," *IEEE Transactions on Antennas and Propagation*, vol. 66, no. 4, pp. 2170–2173, 2018, doi: 10.1109/tap.2018.2801346.

[27] A. Alomainy and Y. Hao, "Modeling and Characterization of Biotelemetric Radio Channel From Ingested Implants Considering Organ Contents," *IEEE Transactions on Antennas and Propagation*, vol. 57, no. 4, pp. 999–1005, 2009, doi: 10.1109/tap.2009.2014531.

[28] S. S. Mosavinejad, P. Rezaei, A. A. Khazaei, and J. Shirazi, "A triple-band spiral-shaped antenna for high data rate fully passive implantable devices," *AEU - International Journal of Electronics and Communications*, vol. 159, p. 154474, 2023, doi: 10.1016/j.aeue.2022.154474.

[29] J. Zhang *et al.*, "A Compact Dual-Band Implantable Antenna for Wireless Biotelemetry in Arteriovenous Grafts," *IEEE Transactions on Antennas and Propagation*, vol. 71, no. 6, pp. 4759–4771, 2023, doi: 10.1109/tap.2023.3266786.

[30] S. Ahmad, B. Manzoor, S. Naseer, N. Santos-Valdivia, A. Ghaffar, and M. I. Abbasi, "X-Shaped Slotted Patch Biomedical Implantable Antenna for Wireless Communication Networks," *Wireless Communications and Mobile Computing*, vol. 2022, pp. 1–11, 2022, doi: 10.1155/2022/7594587.

[31] M. M. Jawad *et al.*, "Implantable slot antenna with substrate integrated waveguide for biomedical applications," *TELKOMNIKA (Telecommunication Computing Electronics and Control)*, vol. 19, no. 5, p. 1450, 2021, doi: 10.12928/telkomnika.v19i5.19952.

BIOGRAPHIES OF AUTHORS

Abdelmouttalib Bousrout 🆔 🇬 SC ◐ received a specialized Master's degree in Telecommunication Systems at Ibn Tofail University in 2021 after earning a Bachelor of Physics degree with an electronics concentration from Cadi Ayyad University in 2018. He is currently pursuing her doctorate in signal processing and telecommunication at Ibn Tofail University in Kenitra, Morocco. Two of his main areas of interest are miniaturization and the development of high-performing antennas for biomedical applications. He can be contacted at email: abdelmouttalib1995@gmail.com.

Asma Khabba 🆔 🇬 SC ◐ obtained a Master of Science in Control, Industrial Computing, Signals, and Systems from Cadi Ayyad University in 2017 after completing her Bachelor of Science in Physics there in 2015. She is currently a Ph.D. candidate at Cadi Ayyad University in Marrakech, Morocco, studying Signal Processing and Telecommunications. Phased arrays, MIMO antennas, millimeter wave and microwave antennas, and 5G antennas are all areas of interest for her study. She can be contacted at email: asma.khabba@edu.uca.ac.ma.

Saida Ibnyaich presently serves as Professor at Morocco's Cadi Ayyad University in Marrakech. She graduated from Cadi Ayyad University in 2002 with a Bachelor's degree in Technical Sciences, in 2005 with a Master's degree in Electrical Engineering with a focus on power electronics and industrial control, and in 2013 with a Doctorate in Computing and Telecommunication. Her areas of interest in research include millimeter waves, PIFA antennas, patch antennas, microwaves, and telecommunications. She can be contacted at email: s.ibnyaich@uca.ac.ma.

Tomader Mazri a permanent member of the Electrical and Telecommunications Engineering Laboratory and a professor at the National School of Applied Sciences of Kenitra. IbnTofail University awarded an HDR degree in networks and telecommunication, Sidi Mohamed BenAbdellah University and INPT of Rabat awarded a Ph.D. degree in Microelectronics and Telecommunication, a Master's degree in Microelectronics and Telecommunication Systems, and Cadi Ayyad University awarded a Bachelor's degree in Telecommunication. She can be contacted at email: tomader.mazri@uit.ac.ma.

Mohamed Habibi he received his State Doctorate Thesis in Electronics from Mohammed University V of Mohammadia Engineering School of Rabat, Morocco, in 1993. He is currently employed by Ibn Tofail University in Kenitra, Morocco, as a member of the Laboratory of Electronic Systems, Information Processing, Mechanics, and Energy. His work focuses on applications using microwaves. He can be contacted at email: habibi.mohamed@uit.ac.ma.

Tole Sutikno is currently employed as a lecturer in the Electrical Engineering Department at Universitas Ahmad Dahlan (UAD), which is located in Yogyakarta, Indonesia. In 1999, 2004, and 2016, he graduated with a Bachelor of Engineering from Universitas Diponegoro, a Master of Engineering from Universitas Gadjah Mada, and a Doctor of Philosophy in Electrical Engineering from Universiti teknologi Malaysia. All three degrees are in the field of Electrical Engineering. Since the year 2008, he has held the position of Professor at the Universitas Ahmad Dahlan in Yogyakarta, Indonesia. He is among the top 2% of researchers named by Stanford University and Elsevier BV as the most influential scientists in the world for 2021-present. His research interests include the areas of digital design, industrial applications, industrial electronics, industrial informatics, power electronics, motor drives, renewable energy, FPGA applications, embedded systems, artificial intelligence, intelligent control, digital libraries, and information technology. He can be contacted at email: tole@te.uad.ac.id.